CFD simulations of active flow control devices applied on a cambered flap

Abderahmane Marouf, Dinh Hung Truong, Yannick Hoarau, Alain Gehri, Dominique Charbonnier, Jan B. Vos, Marianna Braza

AIAA SciTech Forum
January 3-7, 2022, San Diego, CA & Virtual
AIAA SCITECH 2022 Forum

10.2514/6.2022-1545

CFD simulations of active flow control devices applied on a cambered flap

A. Marouf *, H. Truong†, Y. Hoarau‡
University of Strasbourg, ICUBE Laboratory, 2 Rue Boussingault, F-67000 Strassbourg, France

D. Charbonnier§, J.B. Vos¶, A. Gehri‖
CFS Engineering, EPFL Innovation Park, Batiment A, CH-1015 Lausanne, Switzerland

M. Braza**
Institut de Mécanique des Fluides de Toulouse, F-31400 Toulouse, France

Novel techniques to reduce the negative effects of modern aviation on the environment have been studied for several decades. Among these techniques, one can mention the morphing of the lifting surfaces of an aircraft (wing and flaps), which allows to reduce the weight by removing some mechanisms, while optimizing more finely and in a controlled way the shape of the wings and control surfaces during the different flight phases. On the other hand, there are flow control techniques that are developed and used, such as vortex generators and blowing-suction devices, in order to control the structure of the flow on the lifting surfaces, and thus reduce the drag. The present study proposes a coupling of these 2 types of devices, namely the camber of a flap allowing an increase in lift, coupled with Zero Net Mass Flux (ZNMF) devices that will permit a separated flow that might occur with important camber to reattach. The combination of these both devices is investigated using three-dimensional CFD simulations by means of hybrid RANS/LES turbulence modelling.

I. Nomenclature

C_p	=	pressure coefficient
Cd	=	Drag coefficient
Cl	=	Lift coefficient
c	=	chord
dt	=	time step
F^+	=	jet dimensionless frequency
C_μ	=	blowing momentum coefficient
V_{jet}	=	jet velocity magnitude
ρ	=	air density
Re	=	Reynolds number
U_∞	=	streamflow velocity

*Professor Assistant, University of Strasbourg, amarouf@unistra.fr
†Post-Doctoral, University of Strasbourg, dh.truong@unistra.fr
‡Professor, University of Strasbourg, hoarau@unistra.fr
§Senior Scientist, dominique.charbonnier@cfse.ch
¶Director, jan.vos@cfse.ch, Senior AIAA member
‖Senior Scientist, alain.gehri@cfse.ch
**Research Director CNRS, marianna.braza@imft.fr

II. Introduction

In the 21st century, reducing the negative impacts on the environment is one of the main concerns of the aviation industry. These include the reduction in carbon dioxide emission, aircraft noise and fossil fuel burn. Much progress has been made since the year 2000 through the use of novel engines and improved winglets. However, novel concepts are needed to meet the 2050 challenges proposed by the Advisory Council for Aviation Research and Innovation in Europe (ACARE) FlightPath 2050*.

The use of active flow control (AFC) devices is one method that permit to delay or remove flow separations on wings or control surfaces, and over the last 20 years many studies have been made. Cattafesta and Sheplak [1] made a classification of active flow control devices according several criteria, among them the input energy or topology.

Zero Net Mass Flux (ZNMF) devices belong to the category of fluidic devies. The efficiency of ZNMF actuators depends on various parameters of which two key parameters are the dimensionless frequency of the jet $F^+ = f_{jet}c/U_\infty$ and the ratio of the actuator velocity to the free-stream velocity V_{jet}/U_∞ (or the blowing momentum coefficient $C_\mu = I_j/\frac{1}{2}\rho U_\infty^2 c$). I_j is the time-averaged jet momentum.

Seifert [2] performed for the first time experiments to study the effectiveness of synthetic jets at high Reynolds numbers at around 10^7. The active flow control was applied for a NACA0015 without flap and equipped with a 30% chord trailing edge flap deflected at 20°. The study demonstrated the effectiveness of oscillatory blowing for separation control regardless of the Reynolds number. McCormick [3] investigated experimentally the use of a synthetic jet located at 4% chord from the leading edge for control of airfoil separation at $Re = 5 \times 10^5$. The synthetic jet with an oscillation frequency ($F^+ = 1.3$) and jet momentum coefficient ($C_\mu = 0.5\%$) was able to increase the maximum lift coefficient by 25% and mitigate the stall angle by 6°. Tuck et al. [4] conducted experiments of a flow over NACA0015 airfoil ($Re = 1.54 - 3.08 \times 10^4$) with a ZNMF jet located at the leading edge. An increase of 46% in the maximum lift coefficient was obtained under the controlling conditions with $F^+ = 1.3$ and $C_\mu = 0.14\%$. Tang et al. [5] studied the effects of synthetic jet arrays placed at 23% and 43% of the chord on the aerodynamic performance of an LS(1)-0421MOD airfoil at the Reynolds number $Re = 1.2 \times 10^5$. The jet arrays permitted to increase the lift by 27% and to reduce the drag by 19%.

The influence of synthetic jets has also been investigated by many numerical studies on different airfoils. The use of the Reynolds Averaged Navier Stokes (RANS) approach in the application of unsteady jets to an airfoil NACA0012 at high Reynolds number $Re = 8.5 \times 10^6$ was examined in [6]. At a non-dimensional frequency $F^+ \approx 1$, a synthetic jet placed at 1.5% chord with an inclined angle $\alpha = 22°$ can improve the lift by 27%. They also found that the lift was inversely proportional to the blowing momentum coefficient C_μ. By employing an unstructured-grid Large Eddy Simulation (LES) method, the research study [7], analyzed the flow separation over a NACA0015 with synthetic jet control at Reynolds number of 8.96×10^5. The study confirmed the experiments conducted by [8], where the airfoil was installed in a wind tunnel with a synthetic jet at 12% of the chord. About 70% increase in the lift coefficient was obtained with a jet which the momentum coefficient was 1.23%. Kim et al. [9] performed a numerical study to assess the benefits of single and multiple synthetic jets on a NACA23012 airfoil by solving URANS equations at $Re = 2.19 \times 10^6$. In the case of multiple synthetic jets, several jets were arranged side by side to overcome the limit of the jet peak velocity. The study has shown that the jets operating at a frequency $F^+ = 1$ should be placed at the separation point to reach the maximum lift and the effectiveness of the jet was proportional to the jet momentum.

An automatic optimization of flow control devices is a sensitive subject due to the substantial computational resources needed for a high accuracy analysis of unsteady flow, and the possible multi-constraints of the objective function. To the best of our knowledge, there are only a few studies finding optimal parameters of synthetic jets by employing optimization algorithms. In [10] the effects of a synthetic jet located at 12% chord from the leading edge of a NACA0015 airfoil was studied. They used the URANS method to simulate the flow at $Re = 8.6 \times 10^5$ over the airfoil with an angle of attack varying from 12° to 24°. The solver was then coupled with an optimization procedure to find the optimal parameters of the jet. The synthetic jet reached its optimal performance under the conditions of a dimensionless velocity $V_{jet}/U_\infty = 1.72$, a frequency $F^+ = 0.748$ and an angle with respect to the wall $\alpha = 25°$. In [11] the optimal parameters of a synthetic jet in the control flow around the NACA0015 airfoil at the stall angle 13° and the post stall angle 16° was determined. The Navier–Stokes equations for an incompressible two-dimensional flow were solved by a RANS model at $Re = 8.96 \times 10^5$. An optimization method, called Response Surface Methodology (RSM), was then employed to maximize the lift-drag ratio where the optimization parameters were the jet location, the jet frequency and the jet size. According to this study, as the angle of attack increases, the size of the synthetic jet and the frequency should decrease to obtain the optimal performance. Under this circumstance, the optimum synthetic jet

*Flight Path 2050 Europe's Vision for Aviation, Report of the High Level Group on Aviation Research, EUR 098 EN, 2011

location was moving toward the leading edge to delay the flow separation. The synthetic jet was shown to be the most effective at the post-stall angle with a 66% improvement of the lift-drag ratio. Different studies aimed to examine the Active Flow Control effects towards real scale high-lift system and airplanes such as [12] and showed improvements in the aerodynamic coefficients (lift and drag). They used the so-called blowing-suction method through the spanwise direction with a continuous hole. This requires a higher mass flux that can not be achieved using the Zero Net Mass Flux approach, unless an air source is provided from the engine. According to the literature, the most realistic and feasible concepts are proposed in this work. In the context of the Cleansky Fixed wing Aircraft (SFW-ITD) and Green Rotorcraft Integrated Technology Demonstrator (GRG-IT) European projects, different actuators were designed, embedded inside a helicopter fuselage and tested in an experimental wind tunnel [13]. The results obtained in this framework concerning the actuators are that a maximum velocity peak of 80 m/s could be reached. Moreover, the cambering of a high-lift flap thanks to electroactive morphing in the context of the Large Scale (LS) A3xx prototype of the H2020 N° 723402 EU project SMS: "Smart Morphing Sensing for aeronautical configurations", `www.smartwing.org/SMS/EU` was investigated experimentally and numerically. It was shown that an optimal cambering was able to considerably increase lift and to refrain the excessive drag increase due to the thickening of the wing's section through the cambering.

More recently, we studied two-dimensional active control using different strategies of steady blowing, transient blowing and blowing-suction method based on the Zero Net Mass Flux ZNMF similar as piezo-actuators embedded inside the flap of a high-lift system [14]. The AFC was coupled with a morphing flap. [15–17] using the cambering approach. The morphing using the camber approach showed that an intermediate optimal position could increase the aerodynamic efficiency up to 6.7 %. The approach was extended to a real scale airplane during the take-off flight phase and revealed an important improvement on the aerodynamic forces. However, the concept of the cambering using higher deformations associated with higher angles of flap deflections leads to an important increase of the lift, followed by a large separation on the suction side of the flap, resulting in an important increase of the drag and decrease of the aerodynamic efficiency. The study showed that a 2D coupling of both AFC and morphing could reattach the boundary layer, enhance the pressure distribution over both the flap and the wing system and decrease the width of the wake.
In the present work, the role of the Zero Net Mass Flux - ZNMF will be examined for a three-dimensional wing with a constant span in the context of the Active Flow Control for TiltRotor aircraft (AFC4TR) a CleanSky2 European funded H2020 project (2020-2022) `https://www.afc4tr.eu/`. High-Fidelity numerical simulations using URANS and hybrid RANS/LES turbulence modelling are employed using an adapted grid with the chimera patch to better implement AFC actuators in the high-lift system without any re-meshing. Different locations and orientations of the jets are examined by considering the separation line in order to better reattach the flow and to obtain an enhancement of the aerodynamic efficiency.

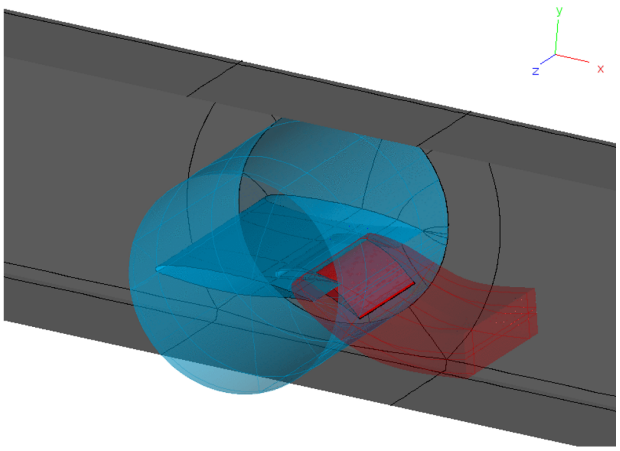

Fig. 1 Computational domain of the high-lift wing-flap system considering the wind tunnel walls

III. Computational setup

A. NSMB solver description

The CFD simulations were carried out using the Navier Stokes Multi Block solver NSMB developed in a consortium composed of different universities and industries [18, 19]. NSMB is a cell-centered finite volume solver using multi block structured grids. Both the patch grid and chimera method are available to simplify the mesh generation for complex geometries. The solver includes a large variety of turbulence models that are standard in the aeronautical industry. For unsteady CFD simulations Hybrid RANS-LES models are available as well as the k-ϵ Organized Eddy Simulation model [20, 21] which were used for 2D and 3D simulations.
The Arbitrary Lagrangian Eulerian (ALE) approach is employed for simulations using moving or deforming grids employed in morphing simulations ([22, 23]). NSMB includes a re-meshing algorithm that is a combination of Volume Spline Interpolation (VSI) [24] and Transfinite Interpolation (TFI).
A specific boundary condition to simulate the movement of the cambering based on different input parameters has been implemented during the Smart Morphing and Sensing "SMS" European funded H2020 project. In an initial step the implementation was made in 2D, and it was assumed that the morphing boundary condition was in a single block only. In later steps this was extended to 3D, and the restriction to have the morphing boundary condition in a single block was removed. Finally, this specific boundary condition was also extended to allow the coupling with the structural movement coming from Smart Memory Alloys (SMAs). When using the morphing boundary condition, NSMB determines automatically the leading and trailing edge as well as the windward and leeward side of the wing or flap. Then for each grid point on this boundary condition it determines the distance to the leading and trailing edge. Together with the input parameters this allows to determine the normal displacement of the grid points on the surface, and the re-meshing algorithm automatically performs the displacement of the grid points into the volume.
The velocity boundary condition implemented to simulate the jet of a ZNMF device reproduces the velocity variation in time (blowing and suction at the surface) obtained by the vibration of a membrane or a piezo actuator as in a hardware device. The parameters of the boundary condition allow for varying the amplitude and the frequency of the velocity fluctuations of the jet.

B. Mesh generation

The ANSYS ICEM CFD pre-processor tool was used to generate the multi-block structured grids needed by the NSMB flow solver.

The sliding mesh approach as well as the Chimera overlapping technique were employed to simplify the mesh generation. Indeed, these techniques allow to create one structured multi block grid for a single configuration, and obtain the other configurations applying only rotations and displacements of partial grid elements (structured blocks) around the moving parts (the flap for example).

To resolve the viscous boundary layer, O-grid topologies with a geometric cell distribution were used closed to the solid walls (wing, flap, wind tunnel, whole aircraft). The first cell height in the wall normal direction was set to obtain a y^+ value close to/below 1 to ensure the proper use of high-Reynolds turbulence modeling, and the growth ratio of the cells normal to the wall was typically close to 1.2. Particular attention was paid also to the refinement of the mesh close to the trailing edge of the wing and the flap which can strongly affect the development of the vortex flow structures in the wakes downstream of these elements, as well as the location of the flow detachment if it occurs.

The morphing of the flap (cambering) has been taken into account during the mesh generation process, by defining a patched area where the specific boundary condition is applied. The Zero Net Mass Flux "ZNMF" devices have been inserted into the flap as an inclined rectangle. Several locations, lengths, diameters and inclination angles of the devices are investigated and a trade-off of the best parameters will be presented in this paper.

An overview of the 2D mesh of the wing and flap configuration investigated is shown in Fig. 2. The bottom and top walls of the wind tunnel have been preserved in the CFD model in order to reproduce as much as possible the characteristics of the flow field in the test section. One can see the sliding area in blue that allows for rotating the main wing to change the angle of attack as in the experimental setup, and the chimera overlapping area in red that permits to change the deflection of the flap. When the morphing of the flap (camber) is imposed, only the red part of the grid is re-meshed to follow the deformation of the flap geometry. The 3D structured grids involve 20 to 40 million cells with local cells refinement downstream of the both trailing edges (wing and flap). The 3D mesh is generated from the 2D mesh by extrusion along the spanwise of the wing and flap.

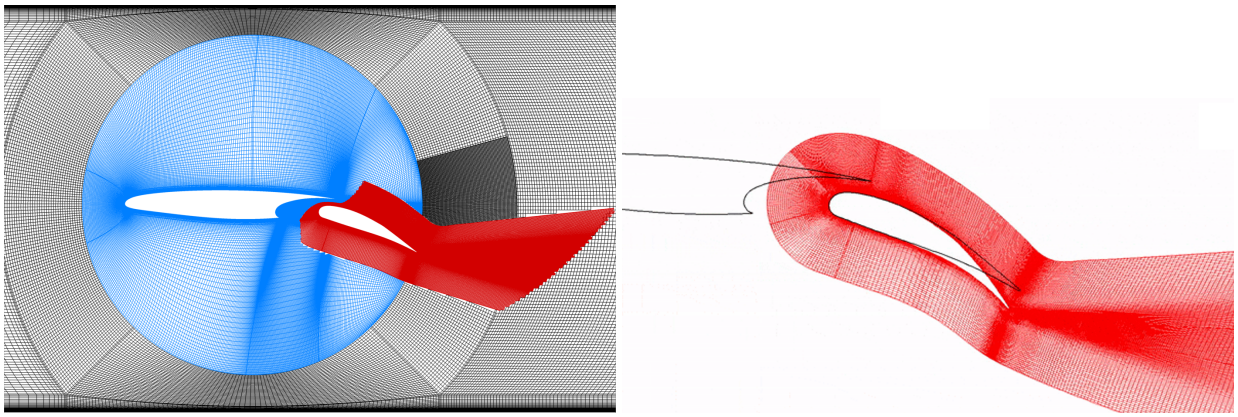

Fig. 2 (left): Multi-block grid using the Chimera method to allow the flap to deflect without any remeshing. (right): the flap cambering compared to the baseline deflected flap at 25°

C. Description of the cases

Different test cases were selected to better understand the effects of the ZNMF on the boundary layer reattachment and to optimize the position of different actuators placed upstream and downstream the separation. In addition, a new concept of oriented jets is proposed.

Fig. 3(A) shows the first test case, a wing with a span of 0.27m. A hybrid Reynolds Averaged Navier-Stokes (RANS)/Large Eddy Simulation (LES) model based on the ideas proposed by Spalart-Allmaras was used. In particular the Delayed Detached Eddy Simulation - Spalart Allmaras "DDES-SA" ([25]) was used as the reference turbulence model. This choice was verified from our previous two-dimensional optimization study [14], where the SA model showed robustness in convergence compared to 2 equations URANS models as for instance the k-ω-SST for the use of Active Flow Control cases in particular at high frequency 100-300Hz and for high jets velocities up to 350 m/s.

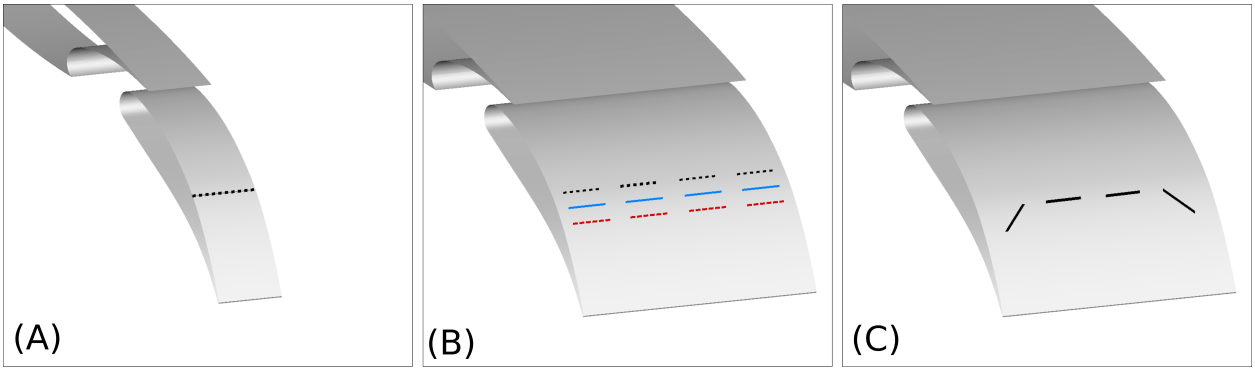

Fig. 3 Set of different test cases selected to examine the ZNMF effects. (A): an adapted case to hybrid modelling DDES-SA with a smaller span. (B) and (C) an adapted cases for URANS modelling to examine the location and orientation effects of the jets regarding the separation line.

In addition, the model was able to predict the flow separation from the higher cambering coupled with high angles of deflection of the flap. The use of hybrid RANS/LES model (DES) is set by the grid cells, so in thicker boundary layer zones, as for instance a presence of a flow separation, the standard DES may be affected by the Modelled Reynolds Stress Depletion issue [26]. To delay the switch to the LES and to treat the entire boundary layer with a URANS model, we use the DDES which provided good results studies for the same configuration at take-off position previously investigated in [15, 27, 28]. A multi-block structured mesh of ≈40 million cells was carefully prepared and adapted to the hybrid model. The implicit dual time stepping approach with a time step of $\Delta t=10^{-5}$ seconds was used to accurately resolve the small scale structures on this adapted grid.

Figure 3(B) presents the second test case with active control jets located along a discontinuous line, the jets are placed at different locations: 50%, 55% and 60% of the flap's chord (indicated by the different color lines). These

positions were selected upstream and downstream of the separation line that is located at approximately 58 % of the flap chord. This grid contains 20 million cells distributed along a constant span of 1m. In real cases where the take-off/landing velocities are important and approximately ≈ equal to the jet velocity, the jet momentum will be not sufficient to delay the separation of the boundary layer and consequently not strong enough to reattach the flow. The French National project ASPIC developed a high efficiency synthetic jet actuator by the Amplified Piezo-Actuator (APA) [29], which can achieve an exit velocity peak of ≈ 150 m/s at an optimal frequency bandwidth. 4 jet actuators are placed

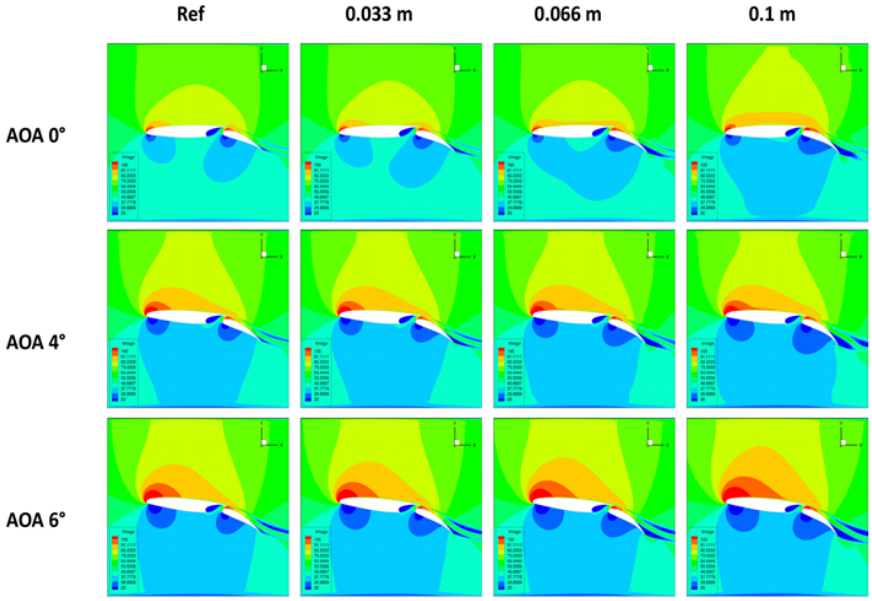

Fig. 4 Mean flow velocity around the Large-Scale (LS) morphing A320 prototype of the SMS project at Mach=0.15 for various angles of attack (each row) and various cambering (each column)

along the spanwise direction on the suction side of the flap. The jets use similar dimensions as of the ASPIC actuator (Fig. 3(B)) with 150mm of width, 1mm of the exit hole and employ an angle of the jet of 45° oriented in the same direction as the flow. As mentioned before they are placed at 3 locations (indicated by the black, blue and red color), that corresponds to locations upstream and downstream of the separation location. A longer span of 1 m using URANS (SA) turbulence modelling approach is employed to better follow the development of the three-dimensional modification of the separation line. Figure 3(C) highlights a new design with two jets placed at the extremities of the flap oriented at 45°. The study will allow to understand the interaction between the jets and their effects on the separation area including coherent vortices.

IV. Results:

A. Morphing using the cambering approach

The morphing using large deformations has been implemented in the NSMB CFD code. The latter is done using special boundary conditions that provide the appropriate movement normal to the flap's surface. The chimera method is needed to quickly change the flap positions as in clean, take-off or landing flight phases without any need for re-meshing. Numerical results were compared and validated with experimental PIV results in the subsonic regime in the context of the Smart Morphing Sensing - SMS project [14]. After that, a large 2D matrix was computed covering different angles of attack [0°- 6°] combined with different cambering positions [0 - 10] cm (Fig. 4). For the baseline case, the flow remains attached for low and intermediate angles of deflection. When the cambering in the lower direction is activated, an important separation occurs near the flap's trailing-edge and moves upstream towards the leading edge. The separation is formed because the flow cannot remain attached for the high deflection angle, which becomes more important when the cambering increases. The separation travels up to 58% when both the angle of attack and the cambering are important.

The cambering increases the curvature of the flap leading to an important flow acceleration on the suction side and a

more predominant bluff body. The aerodynamic lift coefficient is then increased (Fig. 5). The cambering allows a linear improvement of the lift proportional to the increase of the angle of attack. However, due to the more predominant bluff body, the drag is also increased compared to the baseline case. The separation has an important role in this increase, which can be characterized by an important loss of the pressure distribution on the suction side. In addition, the wake's width becomes thicker, which enhances the appearance of the instabilities causing an important non-linear interaction in the different existing shear-layers.

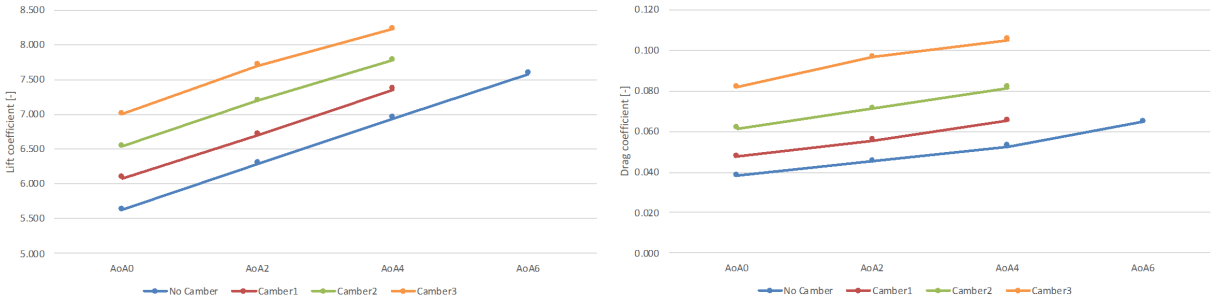

Fig. 5 Lift and drag forces in using different angles of attack and different camber positions in the range [0-10]cm

B. Three-dimensional Active Flow Control "ZNMF" with DDES-SA modelling

The first test case considers a smaller spanwise length (0.27m) using an adapted grid with the hybrid turbulence model DDES-SA. The detached turbulent flow contains smaller chaotic structures that are resolved using the LES model, in addition to the coherent structures considered as large eddies displaying a regular flow pattern in the near area of the trailing edge region. The comparison in Fig. 6(a) shows that the Q-criterion exhibits clearly the flow detachment locations. Anti-clockwise vortices are formed past the flap's trailing edge, due to the high cambering and deflection angle. These vortices extend along the vertical direction through their interactions with the separated upper shear-layer of the flap. These large eddies are presumed as the coherent shedding vortices. The upper and lower shear-layer coming from the wing interact directly with the separation, this will lead to a strengthening of the interaction between the flap's and the wing's shear-layers leading to a considerable growth of the width of the wake. The separation (Fig. 6(a) in blue)

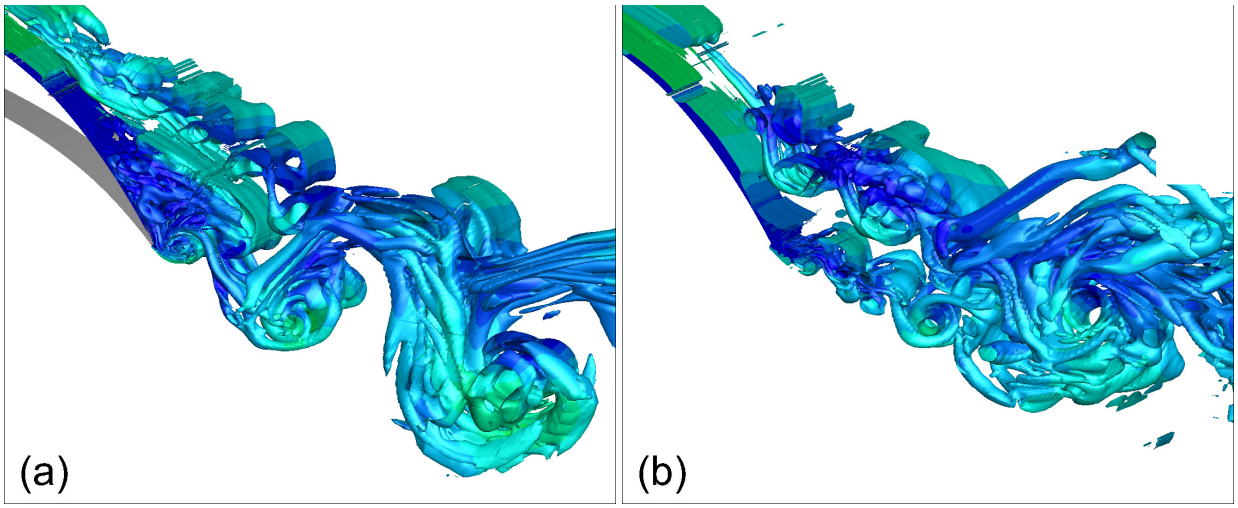

Fig. 6 Snapshot of the Q-criterion showing the region of flow separation in blue (a) located at approximately 58% of the flap's chord and the attenuation of the separation (b) by using the Active Flow Control with ZNMF with the periodic induced blowing-suction jet at a speed of $V_{jet}/U_\infty = 2.9$ and a frequency of F^+=2.38.

located at approximately 58 % of the flap's chord has been attenuated (Fig. 6(b)) in the case of the Active Flow Control with ZNMF by the periodic induced blowing-suction jet at a speed of V_{jet}/U_∞=2.9 and a frequency of F^+=2.38. The injected jet increases the boundary layer momentum thickness. As a result, the separation moves downstream towards the trailing edge. The pressure distribution is enhanced along the separated area of the flap due to the reattachment of the flow.

Both shear-layers of the wing and the flap are highly affected by the ZNMF jet. This last induces a complete disappearance of the anticlockwise vortices formed past the trailing-edge of the flap, because of the reattachment of the flow. The interaction between both shear-layers is then delayed and weakened. The pressure enhancement and the wake thinning will lead to an important modification of the flow behaviour around the high-lift system and will result in improving the aerodynamic efficiency.

C. Three-dimensional Active Flow Control "ZNMF" with (U)RANS modelling

Based on real piezo-actuators and due to the mass-flux limitations, a more realistic configuration has been examined. Four jets with similar dimensions are embedded inside the flap along a spanwise of 1m (Fig. 8). The orientation and location of the jets are easily modified using the Chimera method with an appropriate local refinement. The angle of the jet is an important factor to examine, the study [30] applied in the leading edge area a synthetic jet to reattach the flow. When the jet location is approximately near the separation point, the required momentum coefficient of the jet is decreased. The pressure distribution (on the wing's suction side) as the separation bubble varies in size with the change of the jet angle. However, the study treated leading edge separation in a limited range of Reynolds numbers. The use of Single-Pulse control placed upstream the separation displayed an improvement of the aerodynamic forces [31].

Here the jet is applied at different locations upstream and downstream of the separation line located on the suction

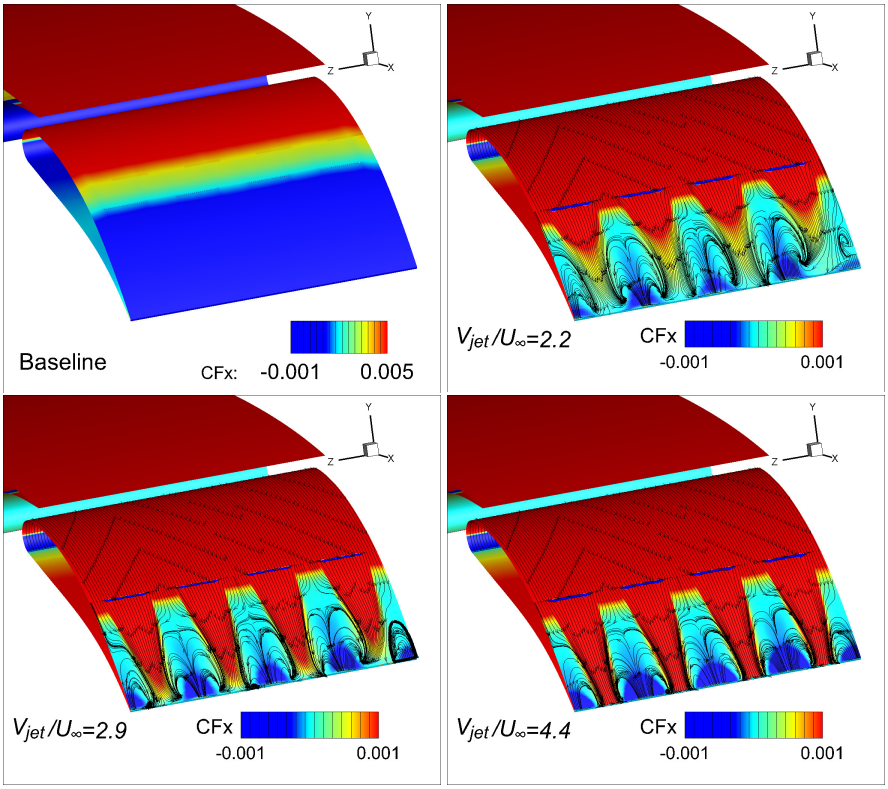

Fig. 7 Contours of the friction coefficient component CF_x for different jet velocities and a comparison with the baseline configuration (morphing through the cambering)

side of the flap, as shown in Fig. 7 using the horizontal component of the friction coefficient CF_x. The blue region represents the separation area. The left and right boundary conditions are considered as symmetry conditions, where the flow field pattern of the solution is mirrored. The fluxes crossing the symmetry are considered null and normal components of variables are forced to zero.

Results of steady simulations are examined using different jet velocities, by taking into account the jet momentum limitation provided by the piezo-actuators. The jets are placed at 60% of the flap's chord. The steady separation control is more effective when the V_{jet}/U_∞ is increased, this can be illustrated by the attenuation of the blue region in Fig. 7 and the flow reattachment that reaches the trailing edge region. The horizontal distances between the actuators allow the formation of two counter rotating vortices enclosed between each two injected jets. Their size and location are controlled by the intensity of the jet. When the jet velocity is fixed at V_{jet}/U_∞=2.2, the counter rotating vortices are less sensitive to the jet, they interact together becoming more energetic and break the jet line by detaching the flow (Fig. 7). As a result, the separation line moves upstream and becomes more significant due to this non-linear interaction between the vortices and the injected jets. When the velocity is set at V_{jet}/U_∞=2.9 or V_{jet}/U_∞=4.4, the momentum of the jet becomes more energetic, suppresses completely the separation and reduces the size of the counter-rotating vortices. However, a steady simulation assumption simulates the effects of only the steady blowing jet and is not considering the periodicity. The effects of the blowing-suction can only be taken into the account by unsteady simulations, and the dynamic interaction between the counter rotating vortices under the periodic effects of the injection of the jet will be examined. Capturing the unsteadiness of the flow permits to resolve the fluctuation fields, which are crucial in the optimisation of the aerodynamic forces during real flight conditions.

In this context, URANS simulations with a jet velocity of V_{jet}/U_∞ = 4.4 and a frequency of F^+=2.6 adopting blowing-suction jets are employed, while considering the limitation of the mass flux of the real piezo-actuators. As previously mentioned, 3 locations are selected 50 %, 55 % and 60 % of the flap's chord. The separation line is located at 58 % following the change in the sign of the friction coefficient CF_x. The control jets don't cause a fully reattachment, because their control effectiveness is limited by the maximum mass flux that can be obtained with the piezo-actuators. This can be explained by the lower induced jet momentum to cause a full reattachment of the boundary layer. Figure.

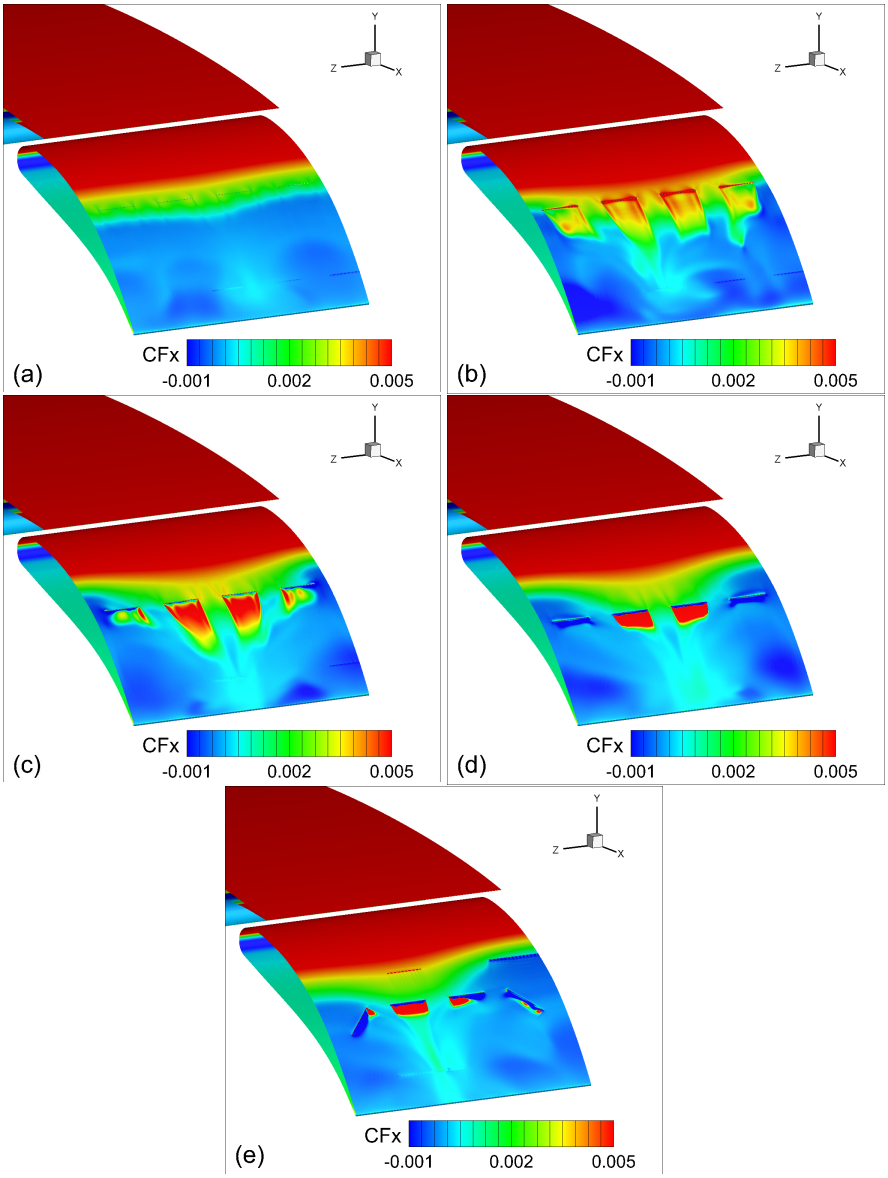

Fig. 8 Unsteady contours of the friction coefficient component CF_x for different jet locations and a comparison with the baseline configuration (morphing through the cambering)

8(a), 8(b) and 8(c) represent the friction coefficient respectively 50%, 55% and 60% of the location of jets. When the jet is placed upstream the separation (Fig. 8(a)) a partial reattachment can be obtained mainly in the middle of the flap. Both central jets N°2 and N°3 are surrounded with corner jets, this will lead to better reattachment in the middle compared to the corners. When the location is set at 55 % (Fig. 8(b)), both corner jets are only partially effective, because the separation line moves upstream to their location. Finally, when the location of the jets is downstream the separation line (Fig. 8(c)), the corner jets loose their effectiveness regarding the reattachment of the flow, because they are fully immersed inside the separation. This will lead to a loss of the pressure distribution compared to the other cases. Figure 8(e) highlights the case (C) mentioned previously. Corner jets are oriented with a fixed angle compared to the case (B) where all the jets are horizontal. A considerable loss in the effectiveness of the separation control is induced using oriented jets, because they are located after the separation line and fully emerged inside the separated region. This configuration tends to be more realistic with the use of Zero Net Mass Flux ZNMF control strategy employing a certain kind of piezo-actuators. However, the separation is not fully controlled due to the limitation of the jet momentum which is related to the mass flux. The latter has an important role in the reattachment of the flow.

V. Conclusions

High-Fidelity numerical simulations have been carried out using the ZNMF approach in the context the European project CleanSky AFC4TR. Morphing with the cambering approach is employed, it consists of deforming the flap up to 10% of its chord in addition to the high deflection angle. An optimal cambering shape has been derived, able to provide a considerable aerodynamic performance increase. The lift force increases with the increase of the camber, due to the important acceleration of the flow that leads to high pressure gradient between both the suction and the pressure surfaces of the flap. The flow control with the ZNMF is exploited to restore and refrain this drag increase by reattaching the flow, while maintaining the lift force higher. The use of the hybrid model DDES-SA applied for a small span wing, revealed the interaction between both the wing and the flap shear-layers. When the ZNMF is applied, the flow reattaches and delays the merging between both shear-layers, which leads to an important wake thinning. In addition, the use of a larger span with URANS modelling permitted to study different locations of real jets, while considering the limitation of the mass flux produced by the existing piezo-actuators. First, a steady blowing with different jet intensities showed an important reattachment. The distance between the jets leads to the formation of two counter rotating vortices. These interact together and with the injected jet. The unsteadiness of the flow reinforce the interaction between these eddies and the separation. This makes the separation to travel upstream. The periodicity of the jet blowing-suction helps also this process compared to the steady blowing. The jets should be installed upstream the separation and should be kept closed to the separation to avoid the jet momentum dissipation. Oriented jets are totally immersed inside the separation leading to a loss of their effectiveness. An optimisation of their locations should be examined in the future.

Acknowledgments

The results presented in this paper are carried in the CleanSky2 project AFC4TR (funded by the European Union H2020 program under Grant Agreement 886718) and the H2020 project SMS (under Grant Agreement 723402). This work was granted access to the HPC resources of [CINES/TGCC] under the allocations 2020-2021-2022-[A0102A11355] and [A0102A05140] made by GENCI. The authors would like to acknowledge the High Performance Computing Center of the University of Strasbourg for supporting this work by providing scientific support and access to computing resources. Part of the computing resources were funded by the Equipex Equip@Meso project (Programme Investissements d'Avenir) and the CPER Alsacalcul/Big Data.

References

[1] L.N., C. I., and M., S., "Actuators for Active Flow Control," *Annual Review Fluid Mechanics*, Vol. 43, No. 1, 2011, pp. 247–272.

[2] Seifert, A., and Pack, L. G., "Oscillatory Control of Separation at High Reynolds Numbers," *AIAA Journal*, Vol. 37, No. 9, 1999, pp. 1062–1071. https://doi.org/10.2514/2.834.

[3] McCormick, D., "Boundary layer separation control with directed synthetic jets," *38th Aerospace Sciences Meeting and Exhibit*, American Institute of Aeronautics and Astronautics, 2000. https://doi.org/10.2514/6.2000-519, URL https://doi.org/10.2514/6.2000-519.

[4] Tuck, A., and Soria, J., "Active flow control over a naca 0015 airfoil using a znmf jet," *The University of Sydney*, 2004, p. 00178.

[5] Tang, H., Salunkhe, P., Zheng, Y., Du, J., and Wu, Y., "On the use of synthetic jet actuator arrays for active flow separation control," *Experimental Thermal and Fluid Science*, Vol. 57, 2014, pp. 1–10. https://doi.org/https://doi.org/10.1016/j.expthermflusci.2014.03.015.

[6] Donovan, J., Kral, L., and Cary, A., "Active flow control applied to an airfoil," *36th AIAA Aerospace Sciences Meeting and Exhibit*, American Institute of Aeronautics and Astronautics, 1998. https://doi.org/10.2514/6.1998-210, URL https://doi.org/10.2514/6.1998-210.

[7] You, D., and Moin, P., "Active control of flow separation over an airfoil using synthetic jets," *Journal of Fluids and Structures*, Vol. 24, No. 8, 2008, pp. 1349–1357. https://doi.org/https://doi.org/10.1016/j.jfluidstructs.2008.06.017.

[8] Gilarranz, J., Traub, L., and Rediniotis, O., "A New Class of Synthetic Jet Actuators—Part II: Application to Flow Separation Control," *Journal of Fluids Engineering-transactions of The Asme - J FLUID ENG*, Vol. 127, 2005. https://doi.org/10.1115/1.1882393.

[9] Kim, S. H., and Kim, C., "Separation control on NACA23012 using synthetic jet," *Aerospace Science and Technology*, Vol. 13, No. 4, 2009, pp. 172–182. https://doi.org/https://doi.org/10.1016/j.ast.2008.11.001.

[10] Duvigneau, R., and Visonneau, M., "Optimization of a synthetic jet actuator for aerodynamic stall control," *Computers and Fluids*, Vol. 35, No. 6, 2006, pp. 624–638. https://doi.org/https://doi.org/10.1016/j.compfluid.2005.01.005.

[11] Montazer, E., Mirzaei, M., Salami, E., Ward, T., Romli, F., and Kazi, S., "Optimization of a synthetic jet actuator for flow control around an airfoil," *IOP Conference Series: Materials Science and Engineering*, Vol. 152, 2016, p. 012023. https://doi.org/10.1088/1757-899X/152/1/012023.

[12] Lehmkuhl, O., Lozano-Durán, A., and Rodriguez, I., "Active flow control for external aerodynamics: from micro air vehicles to a full aircraft in stall," Vol. 1522, 2020, p. 012017. https://doi.org/10.1088/1742-6596/1522/1/012017, URL https://doi.org/10.1088/1742-6596/1522/1/012017.

[13] Ternoy, F., Dandois, J., David, F., and PRUVOST, M., "Overview of Onera Actuators for Active Flow Control," *AerospaceLab*, , No. 6, 2013, pp. p. 1–14. URL https://hal.archives-ouvertes.fr/hal-01184470.

[14] Marouf, A., Chouippe, A., Vos, J. B., Charbonnier, D., Gehri, A., Braza, M., and Hoarau, Y., "Unsteady CFD simulations for Active Flow Control," American Institute of Aeronautics and Astronautics, 2021. https://doi.org/10.2514/6.2021-2854, URL https://doi.org/10.2514/6.2021-2854.

[15] Marouf, A., "Analyse physique de concepts du morphing électroactif pour accroître les performances aérodynamiques des ailes du futur par simulation numérique de Haute Fidélité et modélisation de la Turbulence à nombre de Reynolds élevé," Ph.D. thesis, 2020. https://doi.org/https://www.theses.fr/s18407, URL https://www.theses.fr/s184078, thèse de doctorat dirigée par Hoarau, Yannick et Braza, Marianna, Mécanique Des Fluides, Université de Strasbourg 2020.

[16] Tekap, Y. T. B., Giraud, A., Jodin, G., Nadal, C., Marouf, A., Martinez, I. G., Harribey, D., Nogarede, B., Rouchon, J.-F., and Braza, M., "Design of a Large-Scale High-Lift Morphing A320 Wing Based on Electro-Mechanical Actuators and Shape Memory Alloys," American Institute of Aeronautics and Astronautics, 2019. https://doi.org/10.2514/6.2019-2908, URL https://doi.org/10.2514/6.2019-2908.

[17] Tekap, Y. T. B., Giraud, A., Jodin, G., Nadal, C., Marouf, A., Martinez, I. G., Harribey, D., Nogarede, B., Rouchon, J.-F., and Braza, M., "Design of a Large-Scale High-Lift Morphing A320 Wing Based on Electro-Mechanical Actuators and Shape Memory Alloys," *AIAA Aviation 2019 Forum*, American Institute of Aeronautics and Astronautics, 2019. https://doi.org/10.2514/6.2019-2908, URL https://doi.org/10.2514/6.2019-2908.

[18] Hoarau, Y., Pena, D., Vos, J. B., Charbonnier, D., Gehri, A., Braza, M., Deloze, T., and Laurendeau, E., "Recent Developments of the Navier Stokes Multi Block (NSMB) CFD solver," *54th AIAA Aerospace Sciences Meeting*, 2016. URL 10.2514/6.2016-2056.

[19] Vos, J. B., Charbonnier, D., Ludwig, T., Merazzi, S., Gehri, A., and Stephani, P., "Recent Developments on Fluid Structure Interaction Using the Navier Stokes Multi Block (NSMB) CFD Solver," *35th AIAA Applied Aerodynamics Conference*, American Institute of Aeronautics and Astronautics, 2017. https://doi.org/10.2514/6.2017-4458, URL https://doi.org/10.2514/6.2017-4458.

[20] Hoarau, Y., "Analyse physique par simulation numérique et modélisation des écoulements décollés instationnaires autour de surfaces portantes," Ph.D. thesis, Toulouse, France, 2002. URL http://theses.fr/2002INPT013H, thèse de doctorat dirigée par Braza, Marianna Dynamique des fluides.

[21] Bourguet, R., Braza, M., Harran, G., and Akoury, R. E., "Anisotropic Organised Eddy Simulation for the prediction of non-equilibrium turbulent flows around bodies," *Journal of Fluids and Structures*, Vol. 24, No. 8, 2008, pp. 1240–1251. URL https://doi.org/10.1016/j.jfluidstructs.2008.07.004.

[22] Simiriotis, N., Jodin, G., Marouf, A., Elyakime, P., Hoarau, Y., Hunt, J., Rouchon, J., and Braza, M., "Morphing of a supercritical wing by means of trailing edge deformation and vibration at high Reynolds numbers: Experimental and numerical investigation," *Journal of Fluids and Structures*, Vol. 91, 2019, p. 102676. https://doi.org/10.1016/j.jfluidstructs.2019.06.016, URL https://doi.org/10.1016/j.jfluidstructs.2019.06.016.

[23] Tô, J.-B., Simiriotis, N., Marouf, A., Szubert, D., Asproulias, I., Zilli, D., Hoarau, Y., Hunt, J., and Braza, M., "Effects of vibrating and deformed trailing edge of a morphing supercritical airfoil in transonic regime by numerical simulation at high Reynolds number," *Journal of Fluids and Structures*, Vol. 91, 2019, p. 102595. https://doi.org/10.1016/j.jfluidstructs.2019.02.011, URL https://doi.org/10.1016/j.jfluidstructs.2019.02.011.

[24] Spekreijse, S.P., Prananta, B.B., and Kok, J., "A simple, robust and fast algorithm to compute deformations of multi-block structured grids," 2002.

[25] Shur, M. L., Spalart, P. R., Strelets, M. K., and Travin, A. K., "A hybrid RANS-LES approach with delayed-DES and wall-modelled LES capabilities," *International Journal of Heat and Fluid Flow*, Vol. 29, No. 6, 2008, pp. 1638–1649. https://doi.org/10.1016/j.ijheatfluidflow.2008.07.001, URL https://doi.org/10.1016/j.ijheatfluidflow.2008.07.001.

[26] Spalart, P. R., Deck, S., Shur, M. L., Squires, K. D., Strelets, M. K., and Travin, A., "A New Version of Detached-eddy Simulation, Resistant to Ambiguous Grid Densities," Vol. 20, No. 3, 2006, pp. 181–195. https://doi.org/10.1007/s00162-006-0015-0, URL https://doi.org/10.1007/s00162-006-0015-0.

[27] Marouf, A., Hoarau, Y., Vos, J. B., Charbonnier, D., Tekap, Y. T. B., and Braza, M., "Evaluation of the aerodynamic performance increase thanks to a morphing A320 wing with high-lift flap by means of CFD Hi-Fi approaches," American Institute of Aeronautics and Astronautics, 2019. https://doi.org/10.2514/6.2019-2912, URL https://doi.org/10.2514/6.2019-2912.

[28] Marouf, A., Simiriotis, N., Tô, J. B., Bmegaptche, Y., Hoarau, Y., and Braza, M., "DDES and OES Simulations of a Morphing Airbus A320 Wing and Flap in Different Scales at High Reynolds," Springer International Publishing, 2019, pp. 249–258. https://doi.org/10.1007/978-3-030-27607-2_20, URL https://doi.org/10.1007/978-3-030-27607-2_20.

[29] Eglinger, E., Ternoy, F., Dandois, J., Aigouy, G., Betsch, E., Jaussaud, G., Fournier, M., and Claeyssen, F., "High-performance Synthetic Jet Actuator for Aerodynamic Flow Improvement Over Airplane Wings," ACTUATOR 2018: 16th International Conference on New Actuators, Bremen, Germany, 25–27 June, 2018.

[30] Amitay, M., Parekh, D. E., Smith, D. R., Kibens, V., and Glezer, A., "Aerodynamic flow control over an unconventional airfoil using synthetic jet actuators," *AIAA Journal*, Vol. 39, 2001, pp. 361–370. URL https://doi.org/10.2514/2.1323.

[31] Carusone, A., Sicot, C., Bonnet, J.-P., and Borée, J., "Transient dynamical effects induced by single-pulse fluidic actuation over an airfoil," *Experiments in Fluids*, Vol. 62, No. 2, 2021. https://doi.org/10.1007/s00348-020-03108-0, URL https://doi.org/10.1007/s00348-020-03108-0.